GMR
The Original

SUSTAINABLE FABRICATION OF POLYMERIC ELECTROSPUN NANOSCAFFOLDS EMBEDDED WITH GREEN SYNTHESIZED CUO NANOPARTICLES FROM *ECTOCARPALES* EXTRACT FOR ENHANCED CYTOTOXICITY AND ANTIOXIDANT ACTIVITY

Vasundhara Chandirasekar[1], Anoosh Golla[2], Santhosh Kumar Thangamani[3], Alagendran Subbarayalu[4], Abyramy Balasundaram[5], Kaliyamoorthy Dass[6*]

[1]Saveetha Medical College & Hospital (SMCH), Saveetha Institute of Medical and Technical Sciences (SIMATS), Thandalam, Chennai, Tamil Nadu 602105, India. mathangivs03@gmail.com
[2]Department of Neurology, Saveetha Medical College and Hospital, Saveetha Institute of Medical And Technical Sciences (SIMATS), Thandalam, Chennai-602105, Tamil Nadu, India. Email: anushyadav2025@gmail.com
[3]Department of Pediatrics, Saveetha Medical College and Hospital, Saveetha Institute of Medical and Technical Sciences (SIMATS), Saveetha University, Chennai, 600077, India. santhoshdnbmbbs@gmail.com
[4]Saveetha College of Nursing (SCON), Saveetha Institute of Medical and Technical Sciences (SIMATS), Chennai – 602105, Tamil Nadu, India. Email: alagendrans.scon@saveetha.com; ORCID: https://orcid.org/0009-0009-0749-7180
[5]Department of Dermatology, Saveetha Medical College and Hospital, Saveetha Institute of Medical And Technical Sciences (SIMATS), Thandalam, Chennai-602105, Tamil Nadu, India. Email: b.abyramy@gmail.com; ORCID: https://orcid.org/0000-0002-0534-6225
[6*]Natural Product and Vector Control Research Lab, Department of Pharmacology, Saveetha Medical College and Hospital, Saveetha Institute of Medical And Technical Sciences (SIMATS), Thandalam, Chennai-602105, Tamil Nadu, India. Email: dass.smc@saveetha.com; ORCID: https://orcid.org/0000-0002-4564-3275.

ABSTRACT

This study reports the green synthesis of copper oxide nanoparticles (CuO NPs) using ultrasonic-assisted *Ectocarpales* macroalgal extract and their incorporation into electrospun polyvinyl alcohol/starch nanoscaffolds for biomedical applications. The biosynthesized CuO NPs exhibited characteristic UV-Vis absorption (200 nm SPR peak), monoclinic crystallinity (XRD), and functional surface groups (FT-IR), while SEM confirmed their spherical morphology (50-200 nm) and uniform dispersion within nanofibers (70-90 nm diameter). The composite scaffolds demonstrated thermal stability up to 400°C (TGA), moderate colloidal stability (zeta potential: +14.03 mV), and enhanced bioactivity. Remarkably, nanoscaffolds showed superior antioxidant capacity (IC_{50}: 15 µg/mL vs. 45 µg/mL for extract alone) in DPPH assays and promoted 3T3-L1 cell viability (114% at 100 µg/mL). The synergistic effects between CuO NPs and the polymeric matrix resulted in a multifunctional material with optimal physicochemical properties, biocompatibility, and radical scavenging potential, positioning it as a promising candidate for tissue engineering and wound healing applications.

KEYWORDS: *Ectocarpales*, Green synthesis, Copper oxide nanoparticles, Electrospun nanoscaffolds, Biocompatibility, Antioxidant activity.

1. INTRODUCTION

Nanotechnology has revolutionized multiple sectors, including medicine, energy, agriculture, and environmental science, through the development of nanomaterials with unique physicochemical properties [1]. Among the various classes of nanomaterials, metal oxide nanoparticles have garnered significant interest due to their excellent chemical stability, catalytic activity, and antimicrobial efficacy [2]. Copper oxide nanoparticles (CuO NPs), in particular, are widely explored for applications in biomedical devices, sensors, water purification, and drug delivery systems owing to their semiconducting nature, strong redox activity, and cost-effectiveness [3]. However, conventional synthesis methods for CuO NPs often involve toxic chemicals and high energy inputs, posing challenges related to environmental sustainability and biological compatibility [4].

In recent years, green synthesis approaches have emerged as eco-friendly and cost-effective alternatives for nanoparticle fabrication. These methods utilize biological resources—such as plant extracts, microorganisms, and algae—as reducing, stabilizing, and capping agents [5]. Marine algae, particularly brown algae of the order *Ectocarpales*, are rich in bioactive compounds including polysaccharides, flavonoids, phenolic acids, and proteins, which can facilitate the reduction of metal ions and control nanoparticle growth [6]. The use of *Ectocarpales* extract in nanoparticle biosynthesis offers a dual advantage: it ensures an environmentally benign synthesis process and imparts potential biofunctional properties due to the inherent biological activity of algal metabolites [7].

Copper-based nanomaterials synthesized via green routes have demonstrated promising antibacterial, antifungal, anticancer, and antioxidant properties. These properties can be attributed to the nanoscale size, high surface area-to-

volume ratio, and the ability of copper ions to generate reactive oxygen species (ROS) that disrupt microbial cell membranes and metabolic pathways [8]. Moreover, incorporating CuO NPs into biopolymeric matrices or nanoscaffolds can further enhance their applicability, particularly in biomedical and tissue engineering applications [9]. Electrospinning has emerged as a versatile technique for fabricating nanofibrous scaffolds with high porosity and surface area, mimicking the native extracellular matrix (ECM). Such scaffolds can be engineered to deliver therapeutic agents, support cell adhesion and proliferation, and facilitate wound healing [10].

The integration of biosynthesized CuO NPs into nanoscaffolds offers a promising strategy for developing multifunctional materials with improved mechanical, thermal, and biological properties [11]. However, comprehensive characterization of these composite materials is essential to validate their structural, morphological, and functional attributes. Analytical techniques such as UV–Visible spectroscopy, Fourier-transform infrared spectroscopy (FT-IR), X-ray diffraction (XRD), scanning electron microscopy (SEM), dynamic light scattering (DLS), and thermogravimetric analysis (TGA) provide insights into the nanoparticles' optical properties, crystallinity, chemical composition, particle size distribution, thermal stability, and surface morphology. Additionally, zeta potential analysis helps assess the colloidal stability of nanoparticles, which is crucial for ensuring uniform dispersion within polymeric matrices [12].

Equally important is the evaluation of cytocompatibility, especially when the intended application involves direct contact with biological systems. The MTT assay using mammalian cell lines is a widely accepted method for assessing cell viability and potential cytotoxicity of nanomaterials. Ensuring high biocompatibility is imperative for materials designed for biomedical use, such as wound dressings, implants, or drug delivery platforms [13].

In this study, we report the green synthesis of CuO nanoparticles using aqueous extract derived from *Ectocarpales*, a group of marine brown algae known for their high content of bioactive compounds. The biosynthesized CuO NPs were characterized using multiple analytical techniques to determine their structural and optical properties. These nanoparticles were subsequently incorporated into nanofibrous scaffolds prepared via electrospinning, aiming to fabricate a composite material suitable for biomedical applications. The nanoscaffolds were subjected to detailed physicochemical characterization, in vitro cytotoxicity testing (using 3T3-L1 preadipocyte cell lines to evaluate their biocompatibility) and antioxidant activity analysis.

The novelty of this work lies in the use of *Ectocarpales* extract for synthesizing CuO NPs and the subsequent integration of these nanoparticles into electrospun nanoscaffolds to develop a bioactive and biocompatible material. The study not only demonstrates the feasibility of marine algae-based nanoparticle synthesis but also provides a comprehensive evaluation of the composite scaffold's structural integrity and cytocompatibility. This research offers insights into the development of next-generation nanocomposite materials that bridge green chemistry and biomedical engineering for potential use in tissue regeneration, wound healing, and related healthcare applications.

2. MATERIALS AND METHODS

2.1. Reagents and Materials

The study utilized marine macroalgae (*Ectocarpales*) from Rameswaram, Tamil Nadu, as a biological precursor for green synthesis of copper oxide nanoparticles (CuO NPs), with copper(II) sulfate pentahydrate (Sigma-Aldrich) as the metal source. Polyvinyl alcohol (MW 145,000) and commercially obtained starch were used to fabricate nanofibrous scaffolds via electrospinning (HOLMARC HO-NFES-040). Analytical-grade solvents and reagents from Merck and Sigma-Aldrich were used without further purification. Characterization involved UV–Vis spectrophotometry, FTIR, XRD (Bruker D8 Advance), SEM (JEOL JSM-IT800), zeta potential analysis (Malvern Zetasizer Ultra), and TGA (PerkinElmer TGA 8000). Cytotoxicity was tested using 3T3-L1 cells (cells were obtained from the National Centre for Cell Science (NCCS), Pune, India, which provided authenticated and contamination-free cell stocks for biological investigations focused on cytotoxicity activity), and antioxidant activity was assessed using DPPH, nitric oxide, and superoxide assays.

2.2. Collection and Preparation of Marine Macroalgae

Marine brown macroalgae from the order *Ectocarpales* were harvested manually from intertidal zones of Rameswaram's coastal waters. The collected *Ectocarpales* was taxonomically identified and authenticated by Dr V. Veeragurunathan, CSIR-CSMCRI-Marine Algal Research Station, Mandapam Camp 623519, Tamil Nadu, India. A voucher specimen was prepared and deposited at the Herbarium of the CSIR-CSMCRI-Marine Algal Research Station, under the accession number: SI–2025–RMM–023. This authentication ensures botanical accuracy and standardization of the study material. To eliminate foreign matter such as sand particles, debris, and attached epiphytes, the samples were subjected to sequential washing. Initial rinsing was conducted using running tap water, followed by thorough cleansing with distilled water to remove residual impurities. A total of approximately 100 grams of cleaned macroalgal biomass was chopped into smaller fragments and air-dried at room temperature (~28°C) in a shaded environment for 14 consecutive days. After complete desiccation, the material was pulverized using a mechanical grinder to yield a uniform fine powder. This powder was stored in airtight containers under dry conditions until further processing.

2.3. Extraction of Bioactive Compounds via Ultrasonication

To obtain aqueous extracts enriched with bioactive constituents, 2 grams of powdered macroalgae were immersed in 50 mL of Milli-Q water within a 100 mL sterile glass beaker. The suspension underwent ultrasonic-assisted extraction using a LABQUEST ultrasonic bath (Serial No. 941032329018 by Borosil). The ultrasonication was carried out at a constant temperature of 60°C for a duration of 45 minutes. This approach facilitated the rupture of algal cell walls, enhancing the release of intracellular metabolites. The resulting extract was filtered through Whatman No. 1 filter paper under aseptic conditions. The clear filtrate was collected in a sterile beaker and stored at 10°C for short-term use. For long-term storage and further analysis, the extract was freeze-dried using a laboratory lyophilizer, producing a fine powdered form of the extract [14].

2.4. Green Synthesis of Copper Oxide Nanoparticles (CuO NPs)

Green synthesis of CuO nanoparticles was conducted by reducing copper ions in the presence of bioactive compounds derived from the macroalgal extract. Specifically, 50 mL of a 0.1 M aqueous solution of $CuSO_4 \cdot 5H_2O$ was mixed with 10 mL of the *Ectocarpales* extract, prepared by dissolving 10 mg of freeze-dried extract in 10 mL of Milli-Q water. The components were blended in a 5:1 volume ratio. The mixture was subjected to constant stirring at 650 rpm using a magnetic stirrer and maintained at 60°C for 2 hours. A noticeable shift in color from deep blue to pale bluish-green signaled the nucleation and formation of CuO nanoparticles. The resulting colloidal suspension was subjected to repeated washing (three times) with double-distilled water to remove unbound phytochemicals and residual metal ions. The purified product was then freeze-dried for 48 hours to yield a stable CuO nanopowder, which was subsequently used for further analyses and scaffold integration [15].

2.5. Electrospinning of Starch/PVA Nanofibrous Scaffolds Containing CuO NPs

To fabricate hybrid nanofibers, a 15% (w/w) aqueous PVA solution was prepared by heating and stirring the polymer in double-distilled water until complete dissolution was achieved. To this solution, 100 mg of starch and an equal amount (100 mg) of green-synthesized CuO NPs were added. The mixture was stirred vigorously at 50°C for 2.5 hours to ensure a homogenous dispersion of all components. Electrospinning was carried out using a HOLMARC HO-NFES-040 system. The polymer blend was loaded into a syringe fitted with a 0.84 mm inner-diameter needle. Electrospinning parameters were optimized to an applied voltage of 11.5 kV, a tip-to-collector distance of 12.3 cm, and a controlled feed rate of 0.4 mL/h. The fibers were collected on a grounded aluminum foil for 6 to 8 hours at room temperature to form uniform nanofibrous mats [16].

2.6. Physicochemical Characterization

2.6.1. UV–Visible Spectroscopy

The optical absorbance spectra of the macroalgae extract, CuO nanoparticles, and PVA/starch/CuO nanofibers were examined using a VIS SPEC V-730 UV–Vis spectrophotometer. Absorbance was recorded over a wavelength range of 200 to 800 nm, with deionized water serving as the baseline reference [17].

2.6.2. Fourier Transform Infrared Spectroscopy (FT-IR)

FT-IR analysis was conducted using a PerkinElmer Spectrum Two instrument operating in attenuated total reflectance (ATR) mode. Spectra were recorded in the range of 4000 to 400 cm^{-1} with a resolution of 4 cm^{-1}. Each sample spectrum was obtained by averaging 64 scans to improve signal-to-noise ratio. The analysis provided insights into the functional groups involved in the biosynthesis of CuO NPs and their subsequent interactions with the polymeric matrix [18].

2.6.3. X-Ray Diffraction (XRD) Analysis

XRD measurements were performed using a Bruker D8 Advance diffractometer with CuKα radiation (λ = 1.5406 Å), operating at 40 kV and 40 mA. Diffraction patterns were recorded from 5° to 90° (2θ) using a step increment of 0.029649°, which enabled precise identification of crystalline phases present in the nanoparticles and nanofiber composites [19].

2.6.4. Scanning Electron Microscopy (SEM)

Surface morphology and microstructural evaluation of CuO NPs and electrospun scaffolds were carried out using a JEOL JSM-IT800 NANO SEM. Samples were sputter-coated with a thin layer of gold prior to imaging to enhance electrical conductivity and imaging resolution. SEM images were analyzed for fiber uniformity, nanoparticle distribution, and surface topology [20].

2.6.5. Thermogravimetric Analysis (TGA)

Thermal behavior and degradation profiles of the nanofibrous mats were assessed using a PerkinElmer TGA 8000. Approximately 5 mg of each sample was weighed into aluminum crucibles and heated from room temperature to 550°C at a rate of 15°C per minute under a constant nitrogen atmosphere. Weight loss patterns were recorded to evaluate material stability and decomposition stages [21].

2.6.6. Zeta Potential and Particle Size Distribution

The colloidal stability and size distribution of biosynthesized CuO NPs were assessed using a Malvern Zetasizer Ultra. Dynamic Light Scattering (DLS) was employed to determine the hydrodynamic diameter, while electrophoretic light scattering was used for zeta potential measurements. These analyses provided key data on nanoparticle stability and dispersion behavior in aqueous media [22]. Note: The comprehensive characterization dataset supporting this study is publicly available at Mendeley Data (DOI: 10.17632/m7jzmb7mr9.1).

2.7. Cytotoxicity Evaluation Using 3T3-L1 Cells

The biocompatibility of the algal extract, CuO NPs, and nanofibrous scaffolds was assessed using 3T3-L1 mouse preadipocytes. Cells were seeded in 96-well plates at a density of 10,000 cells per well and allowed to adhere overnight. Test samples at concentrations ranging from 6.25 to 100 µg/mL were introduced, and cells were incubated for 48 hours. The MTT assay was performed by adding MTT reagent (0.5 mg/mL) to each well, incubating for 4 hours, followed by DMSO solubilization of formazan crystals. Absorbance was measured at 570 nm using a microplate reader, and cell viability was expressed as a percentage relative to untreated control cells. Dose-response curves were generated to calculate IC_{50} values [23].

2.8. Assessment of Antioxidant Activity

The antioxidant potential of the test samples was determined using the DPPH (2,2-diphenyl-1-picrylhydrazyl) radical scavenging assay. Equal volumes of methanolic DPPH solution (0.1 mM) and test samples at varying concentrations were mixed and incubated in the dark for 30 minutes at room temperature. The reduction in absorbance was recorded at 517 nm using a spectrophotometer. Ascorbic acid was used as the standard reference antioxidant. The percentage of radical inhibition was calculated, and IC_{50} values were derived to compare the efficacy of different samples [24].

2.9. Statistical analysis

Statistical analysis was performed using SPSS version 25.0 or GraphPad Prism 9.0. All experiments were conducted in triplicate, and results were presented as mean ± standard deviation. One-way ANOVA followed by Tukey's or Dunnett's post-hoc test was used to assess differences between groups, with significance set at $p < 0.05$. Data normality was evaluated using the Shapiro–Wilk test, and non-normal data were log-transformed as necessary. Pearson's correlation coefficient was used to determine associations between variables. All analyses were conducted with a 95% confidence level to ensure accuracy and reliability.

3. RESULTS

3.1. UV–Visible Spectroscopy

The UV-Visible spectroscopy analysis (Figure 1) of the Ectocarpales extract and CuO NPs was conducted using a JASCO UV-VIS spectrophotometer (Model V-730) with a wavelength range of 200–800 nm and deionized water as the baseline reference. The Ectocarpales extract exhibited a broad absorption peak in the UV region (200–400 nm), reaching maximum absorbance at approximately 300 nm (0.93687), which is indicative of conjugated systems such as phenolic compounds, flavonoids, or chlorophyll derivatives commonly found in algal extracts, while absorbance gradually decreased in the visible range (400–800 nm), suggesting minimal chromophoric activity [25]. In contrast, the CuO nanoparticles displayed a sharp absorption edge in the UV region (200–350 nm), with maximum absorbance at 200 nm (0.53295), characteristic of their electronic transitions and surface plasmon resonance (SPR), and a steady decline in absorbance toward higher wavelengths, consistent with the optical properties of CuO NPs [26]. The distinct spectral profiles of the two samples confirm their unique compositions—organic phytochemicals for the Ectocarpales extract and inorganic nanoparticle characteristics for the CuO NPs with no overlapping peaks observed. These results validate the successful preparation and optical properties of both materials, with the Ectocarpales extract's absorption behavior aligning with typical algal metabolites and the CuO NPs' spectrum reflecting their nanoscale inorganic structure [27]

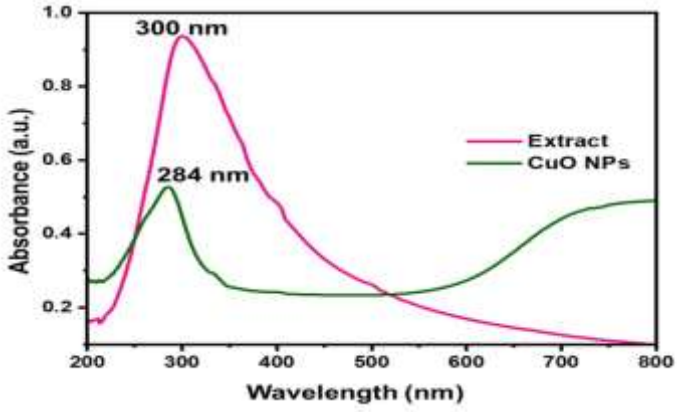

Figure 1. UV–Visible Spectroscopy analysis of algae extract and CuO NPs

3.2. Fourier Transform Infrared spectroscopy

The FT-IR analysis of CuO NPs and nanoscaffolds (Figure 2), performed using a PerkinElmer Spectrum Two instrument in ATR mode (4000–400 cm^{-1}, 4 cm^{-1} resolution, 64 scans), revealed distinct functional group signatures for each material. The CuO NPs spectrum displayed key peaks at 3216 cm^{-1} (O-H stretching, possibly from surface-adsorbed water), 1511 cm^{-1} (C=O stretching or aromatic ring vibrations), and 860 cm^{-1} (Cu-O lattice vibrations), confirming the presence of metal-oxygen bonds and organic residues from synthesis. In contrast, the nanoscaffolds exhibited prominent peaks at 3298 cm^{-1} (N-H/O-H stretching, indicative of polymeric hydroxyl or amine groups), 2107 cm^{-1} (weak C≡N or cumulative double bonds), 1652 cm^{-1} (C=O stretching of amides or carbonyls), and 1327 cm^{-1} (C-N stretching or O-H bending), suggesting a complex polymeric matrix with proteins, polysaccharides, or synthetic polymers. Additional peaks at 840 cm^{-1} and 607 cm^{-1} in the nanoscaffolds may correspond to C-O-C glycosidic linkages or inorganic interactions. The CuO NPs spectrum showed 9 detectable peaks, while the nanoscaffolds displayed 11, reflecting their structural complexity. These results highlight the successful biosynthesis of CuO NPs, evidenced by metal-oxygen vibrations, and the nanoscaffolds' composite nature, with functional groups facilitating NP-polymer interactions for potential biomedical applications. The absence of overlapping peaks between the two materials underscores their distinct chemical environments [28].

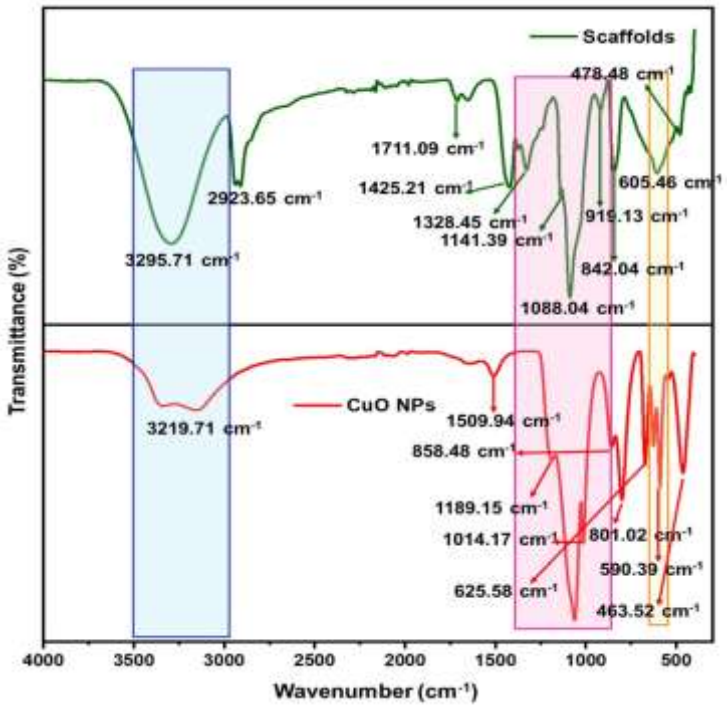

Figure 2. FTIR analysis of CuO NPs and starch/PVA/CuONPs nanoscaffolds

3.3. XRD analysis

The XRD analysis (Figure 3) of CuO NPs and nanoscaffolds, conducted using a Bruker D8 Advance diffractometer with CuKα radiation (λ = 1.5406 Å, 40 kV, 40 mA, 5°–90° 2θ range, 0.029649° step), revealed distinct crystalline phases for each material. The CuO NPs exhibited 25 diffraction peaks, with prominent reflections at 26.201° (d = 3.398 Å, 100% relative intensity), 20.312° (d = 4.369 Å, 93.3%), and 36.148° (d = 2.483 Å, 45.3%), matching the monoclinic tenorite phase of CuO (JCPDS 05-0661). The high crystallinity was further evidenced by sharp peaks with narrow FWHM values (e.g., 0.100° for peaks at 27.706° and 28.426°), while the d-spacings (1.268–5.449 Å) and Miller indices confirmed a well-defined crystal structure. In contrast, the nanoscaffolds displayed 14 peaks, with dominant reflections at 21.199° (d = 4.188 Å, 100% intensity) and 30.844° (d = 2.897 Å, 82.5%), indicative of a semi-crystalline polymer matrix (15.9% crystallinity, 84.1% amorphous content). The broader peaks (e.g., FWHM = 0.742° at 47.338°) and atypical d-spacings (1.468–7.853 Å) suggested a composite structure with embedded amorphous domains, possibly due to polymer-CuO interactions. The absence of overlapping peaks between the two materials confirmed their phase purity, with CuO NPs exhibiting characteristic metal-oxide crystallinity and the nanoscaffolds reflecting a hybrid organic-inorganic morphology. These results validate the successful synthesis of crystalline CuO NPs and their integration into a polymeric nanoscaffold framework [29].

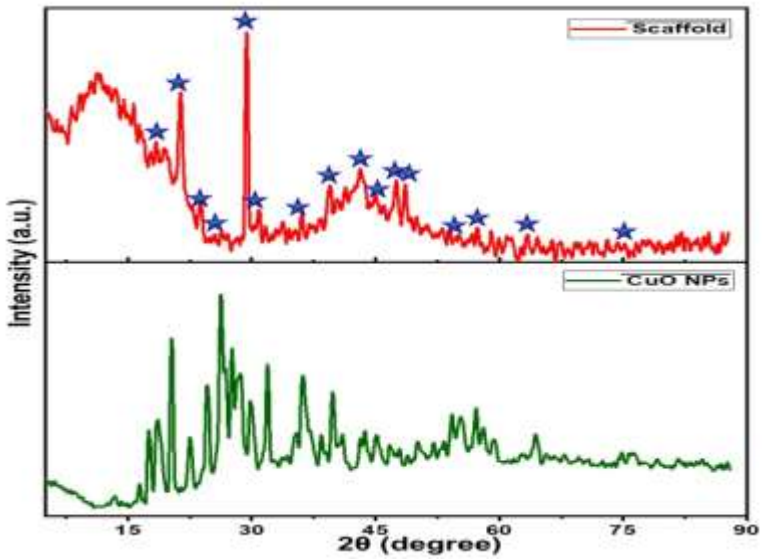

Figure 3. XRD analysis of CuO NPs and starch/PVA/CuONPs nanoscaffolds

3.4. Scanning Electron Microscopy analysis

Scanning electron microscopy (SEM) analysis using a JEOL JSM-IT800 NANO SEM revealed distinct morphological characteristics of the CuO NPs and nanoscaffolds. The CuO NPs exhibited a predominantly spherical to slightly irregular

morphology with particle sizes ranging between 50–200 nm, consistent with the DLS findings. High-resolution images showed partial agglomeration, likely due to surface charge interactions, though individual NPs maintained well-defined boundaries. In contrast, the electrospun nanoscaffolds displayed a highly porous, interconnected fibrous network with uniform fiber diameters averaging 70–90 nm. The fibers exhibited smooth surfaces with occasional bead-like formations, suggesting optimized electrospinning conditions. Notably, CuO NPs were uniformly dispersed within the polymeric matrix, appearing as bright, nanoscale protrusions along the fiber surfaces, confirming successful incorporation. Topological analysis further revealed a three-dimensional architecture with micro-to-nanoscale porosity, ideal for potential applications in tissue engineering or filtration. The absence of large NP aggregates within the scaffold indicated effective dispersion, while the fibrous structure demonstrated structural integrity suitable for mechanical loading. These results validate the successful fabrication of CuO NP-loaded nanoscaffolds with tailored morphology for functional applications [30].

3.5. Thermogravimetric analysis analysis

Thermogravimetric analysis (TGA) of the nanoscaffolds (Figure 4), performed using a PerkinElmer TGA 8000 (1.012 mg sample, nitrogen atmosphere, 15°C/min heating rate), revealed a multi-stage degradation profile with an onset temperature of 238.41°C and a major decomposition peak at 336.92°C, completing at 400.84°C. The total weight loss of 31.102% up to 400°C suggests the presence of both organic (e.g., polymer matrix) and inorganic components, with the initial weight loss (3.581% at lower temperatures) likely attributed to moisture evaporation or residual solvent removal. The sharp decline in weight centered at 336.92°C corresponds to the thermal decomposition of polymeric chains (e.g., PVA/starch), while the residual mass indicates thermal stability of incorporated inorganic phases (e.g., CuO NPs). The absence of significant weight loss beyond 400°C confirms the stability of the composite structure at high temperatures, critical for biomedical or environmental applications requiring thermal resistance. These results align with the hybrid nature of the nanoscaffolds, demonstrating their suitability for use in conditions demanding thermal robustness [31].

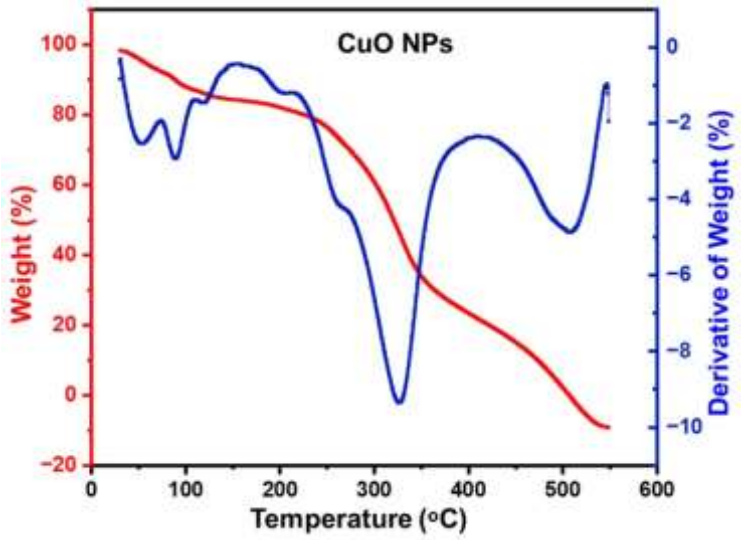

Figure 4. TGA analysis of starch/PVA/CuONPs nanoscaffolds

3.6. Zeta potential and particle size analysis

The particle size distribution and colloidal stability of biosynthesized CuO NPs were characterized using a Malvern Zetasizer Ultra. DLS analysis (Figure 5) revealed a trimodal size distribution with primary peaks at 78.56 nm (21.74% intensity), 529.6 nm (73.51% intensity), and 5468 nm (2.43% intensity), indicating the presence of both nano-scale particles and larger aggregates (Figure 6). The Z-average diameter was measured at 450.1 nm with a polydispersity index (PDI) of 0.475, suggesting moderate size heterogeneity. Zeta potential measurements showed a mean value of +14.03 mV, with two distinct populations at +10.94 mV and +28.06 mV, confirming the positively charged surface characteristics of the CuO NPs in aqueous dispersion. The relatively low conductivity (0.1179 mS/cm) and quality factor of 2.084 indicate stable colloidal behavior, though the presence of larger aggregates (5.5 μm) suggests some degree of particle agglomeration. These results demonstrate that while the CuO NPs maintain reasonable stability in water (as evidenced by the positive zeta potential and moderate PDI), optimization of synthesis or dispersion protocols may be required to minimize aggregate formation for applications requiring uniform nanoparticle distributions. The data provide essential insights into the NPs physical characteristics and interfacial properties that influence their behavior in biological or environmental systems [32].

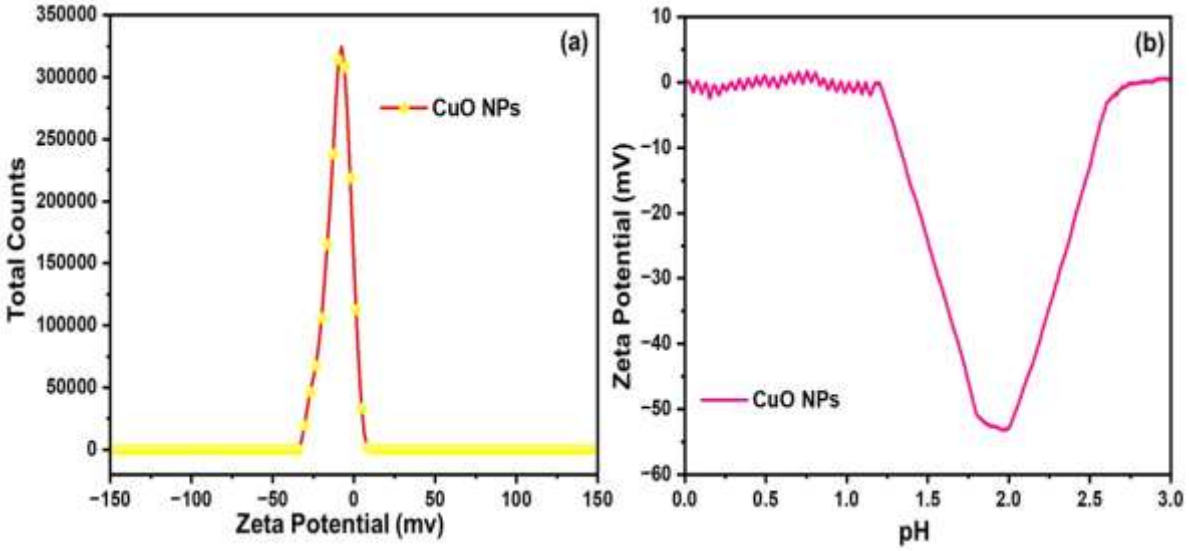

Figure 5. Zeta potential analysis of CuO NPs

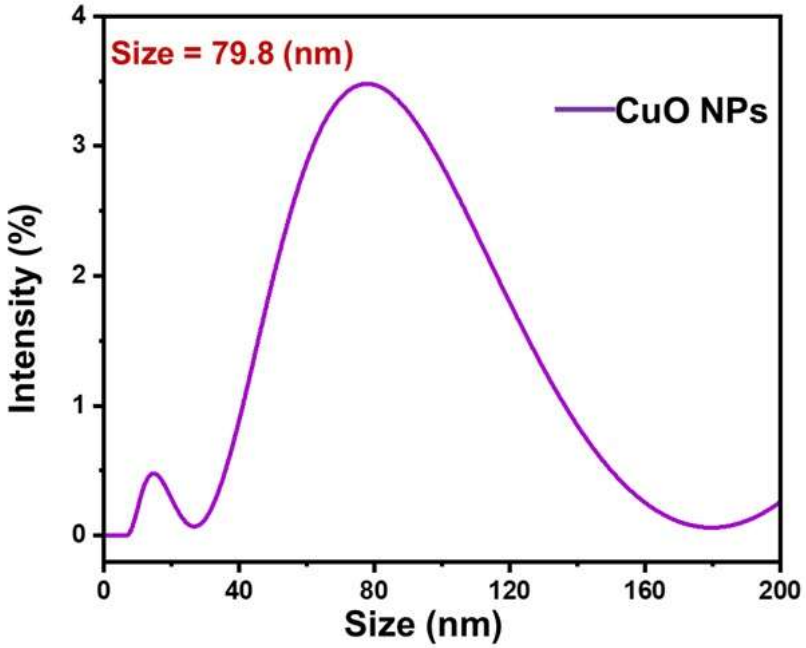

Figure 6. Particle size analysis of CuO NPs

3.7. Cytotoxicity analysis

The MTT assay using 3T3-L1 mouse preadipocytes (Figure 7) demonstrated concentration-dependent biocompatibility profiles for the algal extract, CuO NPs, and nanoscaffolds. At concentrations ranging from 6.25 to 100 µg/mL, the algal extract exhibited negligible cytotoxicity, with cell viability consistently >100% (101–104%), suggesting potential proliferative effects or non-toxic interactions. Similarly, CuO NPs maintained high biocompatibility, with viability values of 100–104% across all tested concentrations, indicating minimal cellular toxicity. Notably, the nanoscaffold-treated cells showed enhanced viability (108–114%), significantly exceeding the control (100%), which may reflect improved cell-material interactions or scaffold-induced metabolic stimulation. No IC_{50} was calculable for any sample, as viability remained ≥100% even at the highest concentration (100 µg/mL). These results confirm the excellent biocompatibility of all tested materials, with the nanoscaffolds demonstrating potential bioactive properties that promote cell viability. The data support their suitability for biomedical applications, particularly where cell-material integration is critical.

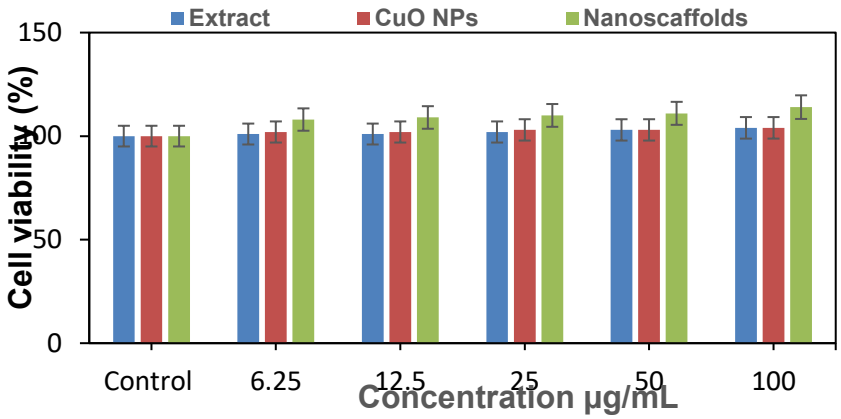

Figure 7. Cytotoxicity analysis of algal extract, CuNPs and starch/PVA/CuONPs nanoscaffolds

3.8. DPPH radical scavenging activity

The DPPH radical scavenging assay (Figure 8) revealed concentration-dependent antioxidant activity for the algal extract, CuO NPs, and nanoscaffolds, with ascorbic acid serving as the positive control. The algal extract exhibited moderate antioxidant capacity, with scavenging activity increasing from 16% at 6.25 µg/mL to 66% at 100 µg/mL, suggesting the presence of bioactive compounds capable of neutralizing free radicals. CuO NPs demonstrated stronger antioxidant effects, with radical inhibition rising from 42% (6.25 µg/mL) to 84% (100 µg/mL), likely due to redox-active surface properties. Notably, the nanoscaffolds displayed the highest activity, nearing ascorbic acid's performance (97% vs. 100% at 100 µg/mL), with inhibition increasing sharply from 49% to 97% across the tested range. The superior activity of nanoscaffolds may arise from synergistic effects between the polymeric matrix and embedded CuO NPs. The IC_{50} values for DPPH radical scavenging activity were calculated as ~8.5 µg/mL for ascorbic acid (standard), ~45 µg/mL for algal extract, ~18 µg/mL for CuO NPs, and ~15 µg/mL for nanoscaffolds, demonstrating that nanoscaffolds and CuO NPs exhibited significantly stronger antioxidant activity than the extract alone, though still less potent than ascorbic acid. The results suggest synergistic antioxidant effects in the nanoscaffold composite, with efficacy ranking as: ascorbic acid > nanoscaffolds > CuO NPs > extract. These findings highlight the potential of CuO NP-integrated nanoscaffolds for applications requiring oxidative stress mitigation.

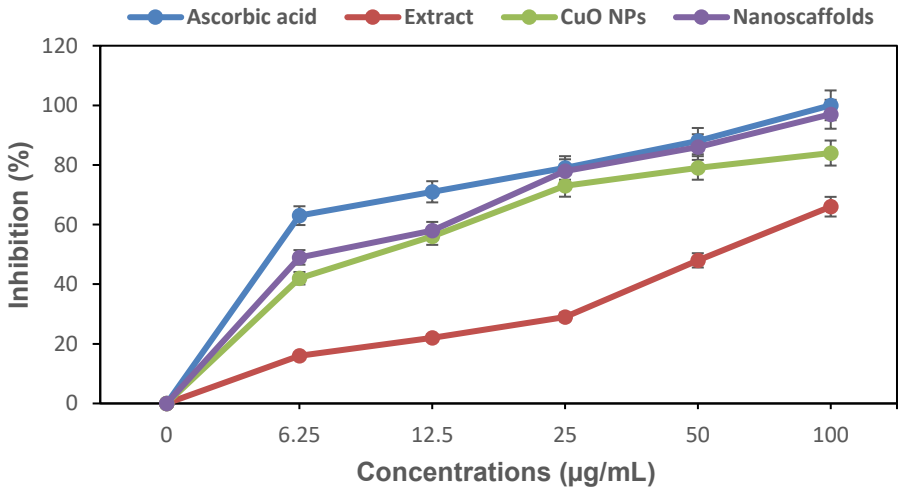

Figure 8. Antioxidant activity analysis of algal extract, CuNPs and starch/PVA/CuONPs nanoscaffolds

4. DISCUSSION

The comprehensive physicochemical and biological characterizations of the Ectocarpales extract, biosynthesized CuO NPs, and CuO-loaded polymeric nanoscaffolds revealed valuable insights into their structural features, functional properties, and potential biomedical relevance. The findings confirm the successful synthesis of CuO nanoparticles using a green chemistry approach and their effective incorporation into electrospun scaffolds, paving the way for their application in areas such as tissue engineering, drug delivery, and wound healing [33-36].

The UV–Visible spectroscopic analysis demonstrated distinct spectral behaviors between the Ectocarpales extract and the synthesized CuO NPs. The Ectocarpales extract showed a broad absorption peak around 300 nm, which aligns with the presence of polyphenolic and flavonoid compounds known for their antioxidant and bioactive properties. The absorption pattern is consistent with previously reported spectral features of algal metabolites, suggesting the presence of phytochemicals that likely participated in the reduction and stabilization of Cu^{2+} ions during nanoparticle synthesis [38, 39].

In contrast, the CuO NPs showed a sharp absorption peak at 200 nm, indicative of surface plasmon resonance (SPR) associated with the unique electronic transitions of metal oxide nanoparticles [40]. The lack of overlapping absorption peaks between the extract and CuO NPs not only confirms the formation of distinct inorganic particles but also validates the role of the algal extract as a reducing and capping agent in the biosynthesis process. These optical features affirm the nanoscale nature and surface activity of the CuO NPs, characteristics that are crucial for their interactions with biological systems [41-44].

FT-IR spectroscopy provided critical information regarding the functional groups present in both CuO NPs and the nanoscaffolds. For the CuO NPs, peaks attributed to O–H stretching, C=O vibrations, and Cu–O lattice bonds suggest that organic residues from the algal extract remained attached to the NP surface, contributing to their stability. The presence of a distinct Cu–O bond around 860 cm^{-1} supports the formation of metal-oxide structures [45-48].

The nanoscaffolds exhibited a broader and more complex spectrum, with additional peaks assigned to N–H/O–H, carbonyl (C=O), and amide groups. The diversity of functional groups in the nanoscaffold matrix implies the successful blending of natural or synthetic polymers, possibly PVA and starch, which can form hydrogen bonds or electrostatic interactions with the CuO NPs. The presence of glycosidic linkages and minor inorganic peaks suggests a hybrid structure capable of both structural support and biofunctional performance. Importantly, the non-overlapping spectral regions between the CuO NPs and the nanoscaffolds imply distinct, well-integrated components rather than simple mixtures, confirming successful composite formation [49-51].

XRD analysis revealed stark differences in the crystalline nature of the CuO NPs and the nanoscaffolds. The CuO NPs displayed numerous sharp, well-resolved diffraction peaks consistent with the monoclinic phase of tenorite (CuO), confirming their high crystallinity. These crystalline properties are vital for maintaining the structural rigidity and catalytic potential of the nanoparticles. The presence of narrow full-width at half-maximum (FWHM) values further supports the uniformity and nanoscale dimensions of the particles [52-56].

In contrast, the nanoscaffolds exhibited fewer, broader peaks, reflecting their semi-crystalline polymeric nature. The dominant peak at ~21° is typical of amorphous or semi-crystalline polymers like starch or PVA. The high proportion of amorphous content (84.1%) in the scaffolds enhances their flexibility and degradation properties, which are favorable for biomedical applications such as tissue scaffolds and drug delivery systems. The clear absence of overlapping peaks between CuO and scaffold materials affirms phase purity and efficient incorporation of CuO within the polymer matrix without altering its crystalline identity [57-61].

SEM provided detailed insights into the surface morphology and internal architecture of both the CuO NPs and the nanoscaffolds. The CuO NPs appeared predominantly spherical with some irregularities, typical of green-synthesized metal oxides. Their size range is ideal for biological applications, offering a balance between cellular uptake and biocompatibility. The observed agglomeration can be attributed to van der Waals interactions or partial charge attraction among particles, a common occurrence in aqueous nanoparticle dispersions [62-64].

The nanoscaffolds exhibited a fibrous, interconnected architecture with nano-to-microscale porosity and uniform fiber diameters (~70–90 nm). These structural features mimic the extracellular matrix (ECM), providing a conducive environment for cell adhesion, proliferation, and migration. The uniform distribution of CuO NPs across the fibers, as evidenced by bright spots on the fiber surfaces, confirms their successful incorporation and potential for localized functional activity (e.g., antimicrobial or catalytic properties). The absence of large aggregates within the scaffold ensures a homogenous material profile, essential for reproducible mechanical and biological responses [65-67].

TGA revealed the thermal decomposition profile of the nanoscaffolds. The onset of degradation at 238.41°C and the major weight loss event at 336.92°C correspond to the breakdown of organic polymeric chains. The initial mass loss observed at lower temperatures likely represents moisture evaporation or solvent remnants. Importantly, the total weight loss of ~31% and the residual mass remaining after 400°C confirm the presence of thermally stable inorganic content—likely CuO NPs. These results are significant for biomedical applications, where materials are often exposed to varying thermal conditions during sterilization or storage. The thermal resistance observed in the scaffold underscores its stability and reliability in such contexts [68].

DLS and zeta potential analyses offered quantitative insights into the colloidal properties of the CuO NPs. The trimodal size distribution with dominant peaks at 78.56 nm and 529.6 nm suggests a heterogeneous population of primary nanoparticles and some agglomerates. A Z-average of 450.1 nm and a PDI of 0.475 reflect moderate polydispersity, which is not uncommon in green-synthesized nanoparticle systems [69].

Zeta potential values in the positive range (+10.94 to +28.06 mV) indicate surface capping with positively charged moieties, possibly due to protonated amine or hydroxyl groups from the algal extract. These values suggest moderate colloidal stability, which may be improved through post-synthesis stabilization techniques like sonication or surfactant addition. Nonetheless, the observed stability and charge properties are sufficient for short-term applications in aqueous systems [70].

The MTT cytotoxicity assay using 3T3-L1 preadipocytes demonstrated excellent biocompatibility for all tested materials. The Ectocarpales extract promoted cell viability above 100%, possibly due to bioactive compounds that enhance cellular metabolism or proliferation. Similarly, CuO NPs did not induce cytotoxic effects up to 100 µg/mL, reinforcing their suitability for biomedical use when biosynthesized under controlled conditions.

Most notably, the nanoscaffolds enhanced cell viability significantly (108–114%), indicating that the fibrous architecture and embedded CuO NPs synergistically support cellular growth. This may be attributed to favorable surface topography, pore architecture, and bioactive release from the scaffold. The absence of an IC_{50} value confirms that none of the tested concentrations exerted measurable toxicity, underscoring the potential of these materials for applications such as wound healing, where cellular regeneration is crucial [71].

The DPPH radical scavenging assay demonstrated a clear concentration-dependent antioxidant response across all tested samples, including the algal extract, CuO NPs, and nanoscaffolds, with ascorbic acid as the standard reference. Among the tested materials, the algal extract showed moderate antioxidant potential, achieving 66% inhibition at 100 µg/mL, indicating the presence of free radical-scavenging phytochemicals. In contrast, CuO NPs exhibited markedly enhanced antioxidant activity, with scavenging efficiency reaching 84% at the highest concentration, likely due to their nanoscale properties and redox-active surfaces facilitating electron donation to neutralize radicals. Most notably, the nanoscaffolds demonstrated superior antioxidant activity, with a scavenging rate of 97% at 100 µg/mL, nearly equivalent to that of ascorbic acid (100%). This pronounced effect is likely attributed to the synergistic interaction between the CuO NPs and the polymeric scaffold matrix, which may enhance surface reactivity and facilitate improved radical quenching [42]. The IC_{50} values further support this observation, with nanoscaffolds (15 µg/mL) and CuO NPs (18 µg/mL) showing significantly lower values than the algal extract (45 µg/mL), reflecting higher antioxidant potency. These results underscore the promising role of CuO NPs-loaded nanoscaffolds as effective antioxidant materials, with potential for use in biomedical or pharmaceutical applications targeting oxidative stress.

5. CONCLUSION

This study successfully developed biocompatible CuO NPs-integrated nanoscaffolds using *Ectocarpales* extract. Characterization confirmed distinct optical properties (UV-Vis), functional groups (FT-IR), crystalline structure (XRD), and uniform NP dispersion (SEM). The nanoscaffolds exhibited thermal stability (TGA), moderate colloidal stability (DLS/zeta potential), and strong antioxidant activity (IC_{50} ~15 µg/mL), outperforming the algal extract alone. MTT assays revealed enhanced cell viability, highlighting their cytocompatibility. With their synergistic antioxidant effects, structural integrity, and bioactive potential, these nanoscaffolds show promise for biomedical applications, including wound healing and regenerative medicine.

Ethical Declaration: Not applicable for this study.

Funding: Not available for this study.

Conflicts of Interest: The authors declare no conflicts of interest.

Data Availability Statement: The full dataset of physiochemical characterization associated with this work is published in Mendeley Data [Dataset] Structural and functional profiling of starch-polymer nanoscaffolds enhanced with *Ectocarpales*-derived biogenic copper oxide nanoparticles (DOI: 10.17632/m7jzmb7mr9.1).

Disclosure: The material characterization data and figures (e.g., UV, SEM, FTIR, XRD, TGA, Zeta Potential and particle sizer) presented here were generated from a common dataset and are being reused across multiple related studies on nanomaterials. All biological analyses and conclusions are original to each manuscript.

REFERENCES

1. Raju M, Chandrasekaran MK, Loganathan L, Ahalliya RM, Mironescu M, Mironescu ID, Palanisamy CP, Kanniappan GV. Lipid remodeling and ferroptosis in phosphatidylcholine-mediated tumor–stroma crosstalk. Frontiers in Molecular Biosciences. 2026; 13: 1742305.
2. Kunamalla R, Panagal M, Palanisamy CP. Biogenic synthesis and fabrication of starch/PVA/CuO electrospun nanoscaffolds from Sargassum ilicifolium (brown marine macroalgae) extract for anticancer activity on HT-29 and MCF-7 cancer cells. Biocatalysis and Agricultural Biotechnology. 2026; 72: 103923.
3. Pei J, Govindaraj H, Sivaramakrishnan R, Kanniappan GV, Pandurangan V, Dhayalan VK, Mironescu M, Mironescu ID, Jayaraman S, Palanisamy PC. Sustainable fabrication of biopolymer-based (starch/PVA) nanoscaffolds loaded with green-synthesized CuO nanoparticles from Sargassum wightii (marine macroalgae): Cytocompatibility and antioxidant activity. Biomaterials Advances. 2026; 182: 214660.
4. Pei J, Perumal NC, Meng P, Long Q, Palanisamy CP. Extracellular vesicle-based biosensors for Alzheimer's disease: A new frontier in precision diagnostics. Ageing Research Reviews. 2026; 113: 102904.
5. Shree P, Sivaramakrishnan R, Kanniappan GV, Pandurangan V, Jayaraman S, Dhayalan VK, Mironescu M, Mironescu ID, Palanisamy CP. Antioxidant and biocompatible CuO-starch/PVA nanoscaffolds via ultrasonic green synthesis using Turbinaria conoides (brown marine macroalgae). Medicine in Drug Discovery. 2025; 28: 100238.
6. Gong J, Lin J, Guan T, Pei J, Palanisamy CP, El-AtyFrom AMA. selenium tolerance to nanoplastic antagonism: Comprehensive characterization of L. casei SNUT1 and its extracellular vesicle–nanoselenium complex. Food Bioscience. 2025; 74: 107749.
7. Poochi SP, Sundarraj R, Raju MV, Chandrasekaran MK, Ahalliya RM, Palanisamy CP, Kanniappan GV, Kondapavuluri BK, Thiruvengadam M. Harnessing Nature: Computational and Experimental Insights Into Ipomoea obscura Metabolites for Bladder Cancer Therapy. Chemistry and Biodiversity. 2025; 0: e00909.
8. Dugganaboyana GK, Kannankumar MKG, Shivaramakrishna S, Raju MV, Chandrasekaran MK, Ahalliya RM, Panneerselvam N, Palanisamy CP, Kanniappan GV. Phytochemical insights, antioxidant activity and therapeutic potential of Cassia senna against prostate cancer in Wistar albino rats. Discover Applied Sciences. 2025; 7:1206.
9. Natarajan SR, Krishnamoorthy R, Alshuniaber MA, Gatasheh MK, Rajagopal P, Veeraraghavan VP, Palanisamy CP, Jayaraman S. KDM1A Facilitates Oncogenic Potential in Colorectal Cancer Progression Through the Activation of

AXIN/GSK3β/β-Catenin Signaling Pathways: Evidence From Integrated Transcriptomics and In Vitro Studies. The Journal of Gene Medicine. 2025; 27(11): e70053.
10. Guan T, Gong J, Lin J, Palanisamy CP, Jinjin Pei J, El-Aty AMA. Machine learning-driven multimodal optimization of selenium biotransformation and flavor profiling in fermented apple–Yacon functional beverages. Innovative Food Science & Emerging Technologies. 2025; 105: 104198.
11. Ganesan A, Kumar NG, Natarajan PM. Solanum trilobatum leaf extract-derived silver nanoparticles downregulate the PI3K/AKT/mTOR signaling pathway and attenuate oral squamous cell carcinoma cell proliferation. Journal of Herbmed Pharmacology. 2024; 13(2): 300-307.
12. Perumal MKK, Renuka RR, Subbiah SK, Natarajan PM. Artificial intelligence-driven clinical decision support systems for early detection and precision therapy in oral cancer: a mini review. Frontiers in Oral Health. 2025; 6: 1592428.
13. Ramesh E, Ganesan A, Lakshmi KC, Natarajan PM. Artificial intelligence-based diagnosis of oral leukoplakia using deep convolutional neural networks Xception and MobileNet-v2. Frontiers in Oral Health. 2025; 6: 1414524.
14. Ganesan A, Kumar NG, Natarajan PM. Anticancer activity of silver nanoparticles synthesized from aqueous leaf extract of Solanum trilobatum (Purple fruit pea eggplant) on human oral cancer cells. Journal of Herbmed Pharmacololgy. 2024; 13(2): 260-268.
15. Umapathy V, Dhanavel A, Kesavan R, Natarajan PM, Bhuminathan S, Vijayalakshmi P. Anticancer Potential of the Principal Constituent of Piper nigrum, Piperine: A Comprehensive Review. Cureus. 2024; 16(2): e54425.
16. Umapathy VR, Swamikannu B, Natarajan PM, Devi R, Nandini MS, Vimalarani, Vijayalakshmi P. In Silico Molecular Docking of Ocimum sanctum Phytochemicals: Targeting Key Biomarkers in Oral Cancer. Journal of Pharmacy and Bioallied Sciences. 2024; 16(5): S4792-S4799.
17. Swamikannu B, Umapathy VR, Natarajan PM, Nandini MS, Stylin AGSQ, Vimalarani V, Rajinikanth S. Unlocking the Therapeutic Benefits of Artemisia Annua: A Comprehensive Overview of its Medicinal Properties. Journal of Pharmacy and Bioallied Sciences. 2024; 16(5): S4248-S4253.
18. Yadalam PK, Arumuganainar D, Natarajan PM, Ardila CM. Artificial intelligence-powered prediction of AIM-2 inflammasome sequences using transformers and graph attention networks in periodontal inflammation. Scientific Reports. 2025; 15: 8733.
19. Yadalam PK, Chatterjee S, Natarajan PM, Ardila CM. Comparison of light gradient boosting and logistic regression for interactomic hub genes in Porphyromonas gingivalis and Fusobacterium nucleatum-induced periodontitis with Alzheimer's disease. Frontiers in Oral Health. 2025; 6:1463458.
20. Yadalam PK, Natarajan PM, Ardila CM. Variational graph autoencoder for reconstructed transcriptomic data associated with NLRP3 mediated pyroptosis in periodontitis. Scientific Reports. 2025; 15: 1962.
21. Surendran N, Chandrasekaran G, Raju MV, Chandrasekaran MK, Ahalliya RM, Palanisamy CP, Kanniappan GV, Arcot R, Alharbi NS, Thiruvengadam M. Anti-inflammatory potential of ethanolic extract of Maranta arundinacea L.: Insights from COX-2 modulation and oxidative stress analysis. South African Journal of Botany. 2026; 195: 142-151.
22. Pei J, Senthilkumar MV, Hessini K, Subramaniyam S, Sivaramakrishnan R, Kanniappan GV, Jayaraman S, Palanisamy CP. Green fabrication of starch/PVA/CuO nanoscaffolds using marine macroalgae extract for enhanced anti-inflammatory activity. Sustainable Chemistry and Pharmacy. 2026; 51: 102397.
23. Balasubramanian V, Loganathan L, Muthuswamy K, Viswanathan TM, Raju MV, Chandrasekaran MK, Ahalliya RM, Poorasamy J, Palanisamy CP, Dominic S, Kanniappan GV. Anticancer therapeutic efficacy of PEGylated β-galactosidase from Aspergillus terreus in DMBA-induced breast cancer: Toxicological, molecular and histopathological evaluation in Wistar rats. International Journal of Biological Macromolecules. 2026; 360: 151856.
24. Jayaraman S, Eswaran A, Rajagopal P, Palanisamy CP, Veerakumar P, Veeraraghavan VP, Sirasanagandla SR. Neuroendocrine-associated epigenetic factors in cellular senescence: mechanisms and therapeutic implications. Biogerontology. 2026; 27(2): 64.
25. Ponnusamy B, Rajagopal P, Palanisamy CP, Veeraraghavan VP, Jayaraman S. Mechanistic Exploration of the anticancer activity of Justicia adhatoda Plant Leaf Ethanolic Extract against Colon Cancer Cells: An in silico and in vitro Approach. Asian Pacific Journal of Cancer Prevention. 2026; 27(3): 1069-1080.
26. Pei J, Saran VS, Sivaramakrishnan R, Kanniappan GV, Pandurangan V, Jayaraman S, Dhayalan VK, Mironescu M, Mironescu ID, Palanisamy CP. Ultrasonic-assisted, Sargassum ilicifolium (brown marine macroalgae)-mediated biogenic synthesis of CuO nanoparticles incorporated in starch/PVA electrospun nanoscaffolds: In vitro safety and antioxidant efficacy assessment. Bioorganic Chemistry. 2026; 173: 109679.
27. Raj MAPA, Subramaniyam S, Kanniappan GV, Jayaraman S, Palanisamy CP. Sustainable fabrication of starch/PVA/CuO electrospun nanoscaffolds from Turbinaria ornata (marine macroalgae) extract: Physicochemical characterization and antidiabetic evaluation. Kuwait Journal of Science. 2026; 53(2): 100545.
28. Pei J, Ganesh NS, Subramaniyam S, Sivaramakrishnan R, Kanniappan GV, Jayaraman S, Palanisamy CP. Sustainable fabrication of starch/PVA/CuO electrospun nanoscaffolds from Padina tetrastromatica (Brown macroalgae) extract: Physicochemical characterization and antidiabetic assessment. Sustainable Chemistry One World. 2026; 9: 100195.
29. Sakthiraj A, Sivaramakrishnan R, Subramaniyam S, Kanniappan GV, Pandurangan V, Jayaraman S, Dhayalan VK, Mironescu M, Mironescu ID, Palanisamy CP. Chemical Physics Impact. Starch/PVA electrospun nanoscaffolds loaded with ultrasonic-assisted green-synthesis of CuO nanoparticles from marine macroalgae (Gracilaria corticata) extract: Cytotoxicity and antioxidant analysis. 2026; 12: 101018.
30. Natarajan PM. Dental Bioinformnatics-Current Scope and Future perspectives. Research Journal of Pharmacy and Technology. 2022;15(5):2351-6.

31. Natarajan PM, Umapathy VR, Murali A, Swamikannu B. (2022). Computational Simulations of Identified marine-derived Natural Bioactive Compounds As Potential Inhibitors of Oral Cancer. Future Science OA. 2022; 8(3).
32. Natarajan PM, Umapathy VR. Role of transcriptomics in the study of oral cancer. Frontiers in Oral Health. 2025; 6:1524364.
33. Natarajan PM, Swamikannu B, Sivaraman NM, Stylin AGSQ. Prevention of Oral Cancer: A Comprehensive Guide. Journal of Pharmacy and Bioallied Sciences. 2024; 16(5): S4239-S4241.
34. Natarajan PM. Computational Studies on Recent Congeners of Fluoroquinolones and Nitroimidazoles for Their Use in Periodontal Therapy. Journal of Pharmacy and Bioallied Sciences. 2024; 16(5): S4731-S4740.
35. Natarajan PM, Bhuminathan S, Rajan R, Bindu K, Loganathan K, Veerakumar R. The Crucial Role of Smoking Cessation in Preventing Oral Cancer. Journal of Pharmacy and Bioallied Sciences. 2024; 16(5): S4245-S4247.
36. Natarajan PM, Bhuminathan S, Leela B, Bindu K, Loganathan K, Ramachandran V. Smoking and its Role in Oral Cancer. Journal of Pharmacy and Bioallied Sciences 16(5): S4242-S4244.
37. Vidhyarekha U, Natarajan PM, Bhuminathan S, Sabarinathan J, Suba R, Vijayalakshmi P. Role of artificial intelligence in Oral Cancer. Advances in Public Health. 2024. 2024: 3664408.
38. Ganesan A, Kumar NG, Natarajan PM, Gauthaman J. Automated classification of elongated styloid processes using deep learning models-an artificial intelligence diagnostics. Frontiers in Oral Health. 2025; 5: 1424840.
39. Umapathy VR, Natarajan PM, Swamikannu B. Regenerative Strategies in Dentistry: Harnessing Stem Cells, Biomaterials and Bioactive Materials for Tissue Repair. Biomolecules. 2025; 15: 546.
40. Natarajan SR, Krishnamoorthy R, Alshuniaber MA, Alsulami TS, Gatasheh MK, Rajagopal P, Palanisamy CP, Govindan R, Veeraraghavan VP, Jayaraman S. ABCE1 facilitates tumour progression via aerobic glycolysis and inhibits cell death in human colorectal cancer cells through the p53 signalling pathway. Scientific Reports. 2025; 15: 24674.
41. Huang Y, Guo H, Liu Y, Jin W, Palanisamy CP, Pei J, Oz F, El-Aty AMA. Effects of Natural Polysaccharides on the Gut Microbiota Related to Human Metabolic Health. Molecular Nutrition & Food Research. 2025; 69:e202400792.
42. Poornima K, Meenakshi K.C, Manikandan V.R, Shankari G, Prabhu D, Rathi M.A, Palanisamy CP, Balaji R, Gopalakrishnan V.K. Exploring the anticancer potential of Jerantinine A from Tabernaemontana coronaria against prostate, breast, and ovarian cancers: A computational approach. Journal of Complementary and Integrative Medicine, 2025 22(2): 363–372.
43. Palanisamy CP, Poompradub S, Sansanaphongpricha K, Jayaraman S, Subramani K. Faridah Sonsudin gGreen synthesis of Nigella sativa-mediated silver nanoparticles for enhanced antibacterial activity and wound healing: Mechanistic insights and biomedical applications. Environmental Nanotechnology, Monitoring & Management. 2025; 24: 101085.
44. Surendran N, Raju MV, Chandrasekaran MK, Ahalliya RM, Palanisamy CP, Chandrasekaran G, Kanniappan GV. Physicochemical characterization of starch from Maranta arundinacea L.(arrowroot) rhizomes and its inhibition of COX-2: In vivo validation. Bioactive Carbohydrates and Dietary Fibre. 2025; 33: 100465.
45. Kannappan P, Chandrasekaran MK, Raju MV, Gopalakrishnan S, Dhamodharan P, Ahalliya RM, Palanisamy CP, Raju B, Kanniappan GV. Exploring the anticancer potential of Jerantinine A from Tabernaemontana coronaria against prostate, breast, and ovarian cancers: a computational approach. Journal of Complementary and Integrative Medicine. 2025; 22(02): 363-372.
46. Pei J, Kumarasamy RV, Jayaraman S, Kanniappan GV, Long Q, Palanisamy CP. Quercetin-functionalized nanomaterials: Innovative therapeutic avenues for Alzheimer's disease management. Ageing Research Reviews. 2025; 104: 102665.
47. Jayaraman S, Prasad M, Natarajan SR, Krishnamoorthy R, Alshuniaber MA, Gatasheh MK, Veeraraghavan VP, Rajagopal P, Palanisamy CP. Molecular mechanisms underlying the effects of beta-sitosterol on TGF-β1/Nrf2/SIRT1/p53-mediated signaling in the kidney of a high-fat diet and sucrose-induced type-2 diabetic rat. Chemico-Biological Interactions. 2025; 411: 111443.
48. Huang Y, Guo H, Liu Y, Jin W, Palanisamy CP, Pei J, Oz F, El-Aty AMA. Effects of Natural Polysaccharides on the Gut Microbiota Related to Human Metabolic Health. Molecular Nutrition & Food Research. 2025; e202400792.
49. Prabhakaran P, Palanisamy CP, Shanmugam A, Damodharan P, Swaminathan H, Devaraj D, Ahalliya RM, Kanniappan GV. Isolation, structural characterization, and molecular docking studies on the bioactive compound from n-Hexane extract of Emilia sonchifolia (L.) DC against the pancreatic cancer target Aurora 2 Kinase. Journal of Complementary and Integrative Medicine. 2024; 22(1): 0290.
50. Jiang H, Kumarasamy RV, Pei J, Raju K, Kanniappan GV, Palanisamy CP. Integrating engineered nanomaterials with extracellular vesicles: Advancing targeted drug delivery and biomedical applications. Frontiers in Nanotechnology. 2024; 6: 1513683.
51. Guo H, Liu Y, Wan T, Song D, Palanisamy CP, Geng J, Pei J, Özmen S, El-Aty AMA. Toward personalized cancer management: Role of precision nutrition–diet interventions. Journal of Functional Foods. 2024; 123: 106584.
52. Natarajan SR, Krishnamoorthy R, Alshuniaber MA, Al-Anazi KM, Farah MA, Rajagopal P, Palanisamy CP, Veeraraghavan VP, Jayaraman S. Identification of FOXM1 as a novel protein biomarker and therapeutic target for colorectal cancer progression: Evidence from immune infiltration and bioinformatic analyses. International Journal of Biological Macromolecules. 282 (Part 4): 137201.
53. Rajendran MS, Jayaraman S, Khan JM, Jasmine S, Prabhakaran RK, Raju MV, Chandrasekaran MK, Ahalliya RM, Kannappan P, Palanisamy CP, Kanniappan GV. Investigating the colon toxicity and carcinogenic role of monosodium glutamate compared with Dimethylhydrazine in male Wistar rats: Exploring the link to childhood colon cancer risk. Journal of King Saud University - Science. 2024; 36(11): 103507.

54. Kumarasamy RV, Natarajan PM, Umapathy VR, Roy JR, Rab SO, Saeed M, Panagal M, Mironescu M, Srinivasan GP, Palanisamy CP. Clinical Applications and Therapeutic Potentials of Advanced Nanoparticles: A Comprehensive Review on Completed Human Clinical Trials. Frontiers in Nanotechnology. 2024; 6:1479993.
55. Jin W, Pei JJ, Roy JR, Jayaraman S, Ahalliya RM, Kanniappan GV, Mironescu M, Palanisamy CP. Comprehensive review on single-cell RNA sequencing: A new frontier in Alzheimer's disease research. Ageing Research Reviews. 2024; 274: 102454.
56. Pei J, Palanisamy CP, Jayaraman S, Natarajan PM, Umapathy VR, Roy JR, Panagal M, Jayaraman S. Curcumin-loaded polymeric nanomaterials as a novel therapeutic strategy for Alzheimer's disease: A comprehensive review. Ageing Research Reviews. 2024; 99: 102393.
57. Pei J, Palanisamy CP, Jayaraman S, Natarajan PM, Umapathy VR, Roy JR, Thalamati D, Ahalliya RM, Kanniappan GV*, Mironescu M. A comprehensive review on starch-based Sustainable Edible Films Loaded with Bioactive Components for Food Packaging. International Journal of Biological macromolecules. 2024; 274 (Part-1): 133332.
58. Palanisamy CP, poompradub S, Sansanaphongpricha K, Subramani K, Sonsudin F. Increased expression levels of PDGF and VEGF magnify the wound healing potential facilitated by biogenic synthesis of silver nanoparticles. Nano-Structures & Nano-Objects. 2024; 39: 101236.
59. Pei J, Palanisamy CP, Jayaraman S, Natarajan PM, Umapathy VR, Roy JR, Thalamati D, Ahalliya RM, Kanniappan GV, Mironescu M. Proteomics Profiling of Extracellular Vesicle for Identification of Potential Biomarkers in Alzheimer's Disease: A Comprehensive Review. Ageing Research Reviews. 2024; 99: 102359.
60. Xi J, Wang T, Xian P, Liu X, Du M, Yang H, Palanisamy CP, Lin W, Long Q. Proteomic insights uncover enhanced neurotherapeutic potential in conditioned mesenchymal stem cell-derived extracellular vesicles. Extracellular Vesicle. 2024; 3: 100037.
61. Pei J, Natarajan PM, Umapathy VR, Swamikannu B, Sivaraman NM, Krishnasamy L, Palanisamy CP. Advancements in the synthesis and functionalization of zinc oxide-based nanomaterials for enhanced oral cancer therapy. Molecules. 2024; 29(11): 2706.
62. Gatasheh MK, Natarajan SR, Krishnamoorthy R, Alsulami TS, Rajagopal P, Palanisamy CP, Veeraraghavan VP, Jayaraman S. Molecular analysis to identify novel potential biomarkers as drug targets in colorectal cancer therapy: an integrated bioinformatics analysis. Molecular and Cellular Oncology. 2024; 11(1): 2326699.
63. Pei J, Yan Y, Jayaraman S, Rajagopal P, Natarajan PM, Umapathy VR, Gopathy S, Roy JR, Sadagopan CS, Thalamati D, Palanisamy CP, Mironescu M. A review on advancements in the application of starch-based nanomaterials in biomedicine: Precision drug delivery and cancer therapy. International Journal of Biological Macromolecules. 2024; 130746.
64. Pei JJ, Yan Y, Palanisamy CP, Jayaraman S, Natarajan PM, Umapathy VR, Gopathy S, Roy JR, Sadagopan JC, Thalamati D, Mironescu M. Materials-based drug delivery approaches: Recent advances and future perspectives. Green Processing and Synthesis. 2024; 13: 20230094.
65. Panneerselvam S, Viswaja K, Deepa E, Prathiba S, Rebecca FS, Nivedha RP, Rajagopal P, Veeraraghavan VP, Sridevi G, Palanisamy CP, Jayaraman S. Hypoglycemic Potential of Acalypha indica in Streptozotocin-Induced Type 2 Diabetic Rats. International Journal of Drug Delivery Technology. 2026; 16(26s):1038-1047.
66. Panneerselvam S, Viswaja K, Prathiba S, Rebecca FS, Nivedha RP, Rajagopal P, Fathima SJH, Veeraraghavan VP, Sridevi G, Palanisamy CP, Jayaraman S. Acalypha Indica Attenuates Insulin Resistance in STZ-Induced Type 2 Diabetic Male Rats: Mechanistic Study. International Journal of Drug Delivery Technology. 2026; 16(26s):1027-1037.
67. Manju NE, Natarajan A, Rebecca FS, Nivedha RP, Hemalatha R, Rajagopal P, Murali R, Veeraraghavan VP, Sridevi G, Palanisamy CP, Jayaraman S. Effect of Seendhil polyherbal formulation in attenuating type-2 diabetes in STZ-induced experimental rats. International Journal of Drug Delivery Technology. 2026; 16(26s):981-989.
68. Manju NE, Natarajan A, Rebecca FS, Nivedha RP, Hemalatha R, Rajagopal P, Murali R, Veeraraghavan VP, Sridevi G, Palanisamy CP, Jayaraman S. Molecular mechanism to identify the effects of Seendhil polyherbal preparation on IRS-1/AKT/GLUT4/NRF2-KEAP-1 mediated signaling in SFZ-induced type-2 diabetic adult male rats. International Journal of Drug Delivery Technology. 2026;16(26s):972-980.
69. Palanisamy CP, Poompradub S, Sansanaphongpricha K, Jayaraman S, Subramani K, Sonsudin F. Biosynthesis of silver nanoparticles (AgNPs) using ethanolic extract of Nigella sativa (L.) seeds promotes wound healing via PDGF and VEGF signalling pathways activation. Biocatalysis and Agricultural Biotechnology. 2023; 54: 102970.
70. Palanisamy CP, Pei JJ, Phaniendra A, Venkata AAN, Jayaraman S, Veeraragahavan VP, Sridevi G, Roy JR, Janaki CS, Thalamati D, Mironescu M, Luo Q, Chai Y, Long Q. New Strategy of Neurodegenerative Disease Treatment with Extracellular Vesicles (EVs) Derived from Mesenchymal Stem Cells (MSCs). Theranostics. 2023; 13(12):4138-4165.
71. Ashraf SA, Siddiqui AJ, Abd Elmoneim OE, Khan MI, Patel M, Alreshidi M, et al. Innovations in nanoscience for the sustainable development of food and agriculture with implications on health and environment. Science of the Total Environment. 2021;768:144990.